



Showcasing research from the Department of Chemical Sciences, University Federico II, Naples, Italy.

The anticancer peptide LL-III alters the physico-chemical properties of a model tumor membrane promoting lipid bilayer permeabilization

The biophysical investigation of the action mechanism of anticancer peptides is crucial for the development of more effective compounds. In this work the interaction of the peptide LL-III with a lipid bilayer containing the anionic lipid phosphatidylserine was characterized, for the first time, in the presence of a physiological concentration of  $\text{Ca}^{2+}$ . The results shed light on the nature of the LL-III selective interaction with the tumor cell membrane.

As featured in:




See Luigi Petraccone *et al.*,  
*Phys. Chem. Chem. Phys.*,  
2023, **25**, 3639.



Cite this: *Phys. Chem. Chem. Phys.*,  
2023, 25, 3639

# The anticancer peptide LL-III alters the physico-chemical properties of a model tumor membrane promoting lipid bilayer permeabilization†

Marco Campanile, Rosario Oliva, Gerardino D'Errico, Pompea Del Vecchio and Luigi Petraccone \*

LL-III is an anticancer peptide and has the ability to translocate across tumor cell membranes, which indicates that its action mechanism could be non-membranolytic. However, the exact mechanism through which the peptide gains access into the cell cytoplasm is still unknown. Here, we use a plethora of physico-chemical techniques to characterize the interaction of LL-III with liposomes mimicking the lipid matrix of the tumor cell membrane and its effect on the microstructure and thermotropic properties of the membrane. Furthermore, the effect of the presence of  $\text{Ca}^{2+}$  cations at physiological concentration was also investigated. For comparison, the interaction of LL-III with liposomes mimicking the normal cell membrane was also studied. Our results show that the peptide selectively interacts with the model tumor cell membrane. This interaction does not disrupt the lipid bilayer but deeply alters its properties by promoting lipid lateral reorganization and increasing membrane permeability. Overall, our data provide a molecular level description of the interaction of the peptide with the model tumor membrane and are fully consistent with the non-membranolytic action mechanism.

Received 1st August 2022,  
Accepted 7th December 2022

DOI: 10.1039/d2cp03528f

rsc.li/pccp

## 1. Introduction

Cancer is a group of diseases characterized by excessive and uncontrolled proliferation of cells and represents one of the major causes of human death.<sup>1</sup> The currently available treatments are based on radiotherapy, chemotherapy and surgery which can lead to a plethora of side effects, mainly due to the lack of specificity.<sup>2</sup> In the search for more effective and selective therapeutics, interest has been developed towards host defense peptides (HDPs), a class of natural compounds identified in most living organisms as the first line of defense of the innate immune system against a broad range of pathogens such as bacteria, virus and fungi.<sup>3</sup> HDPs were historically investigated mainly for their potential application as antimicrobial agents to address the problem of antibiotic resistance. However, after the discovery of the potent antitumor activity of rabbit macrophage peptides MCP-1 and MCP-2 in 1985, an increasing number of peptides were shown to selectively target tumor cells and thus classified as anticancer peptides (ACPs).<sup>4</sup> Most of these peptides act by inducing cell membrane disruption but some of them can translocate into the cytoplasm, where they interact

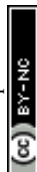
with intracellular targets. However, the exact action mechanism of ACPs is still under debate and several models have been proposed to describe it; nonetheless, a major role is known to be played by the tumor membrane lipid matrix.<sup>5</sup> Indeed, different from healthy eukaryotic cells, malignant cells are characterized by a net negative charge on the external surface. Cell transformation involves, in fact, a loss of membrane asymmetry due to the exposure of the outer leaflet of the anionic lipid phosphoserine (PS), a lipid which is exclusively located in the inner leaflet under physiological conditions.<sup>6</sup> The exposure of PS molecules allows the interaction of their head groups with substances contained in the extracellular matrix such as calcium ions. Previous studies have shown that  $\text{Ca}^{2+}$  is mainly attracted by negatively charged membranes containing PS.<sup>7,8</sup> It has been shown that the preferential coordination of  $\text{Ca}^{2+}$  to this lipid head group alters the physicochemical properties of the lipid bilayer by increasing the rigidity and lipid packing and inducing membrane thickening.<sup>9</sup>

The antimicrobial and anticancer peptide LL-III (VNWKILGKIIKVVK) is a member of the family of *Lasioglossins*, three bioactive peptides extracted from the venom of the bee *Lasioglossum laticeps*. It is an amphipathic pentadecapeptide characterized by a naturally amidated N-terminus and a net charge of +6 below pH 7.4 (Fig. 1).

Previous studies showed that LL-III exhibits a low toxicity towards healthy eukaryotic cells and is active *in vitro* against

Department of Chemical Sciences, University of Naples Federico II, Via Cintia 4,  
80126 Naples, Italy. E-mail: luigi.petraccone@unina.it

† Electronic supplementary information (ESI) available. See DOI: <https://doi.org/10.1039/d2cp03528f>



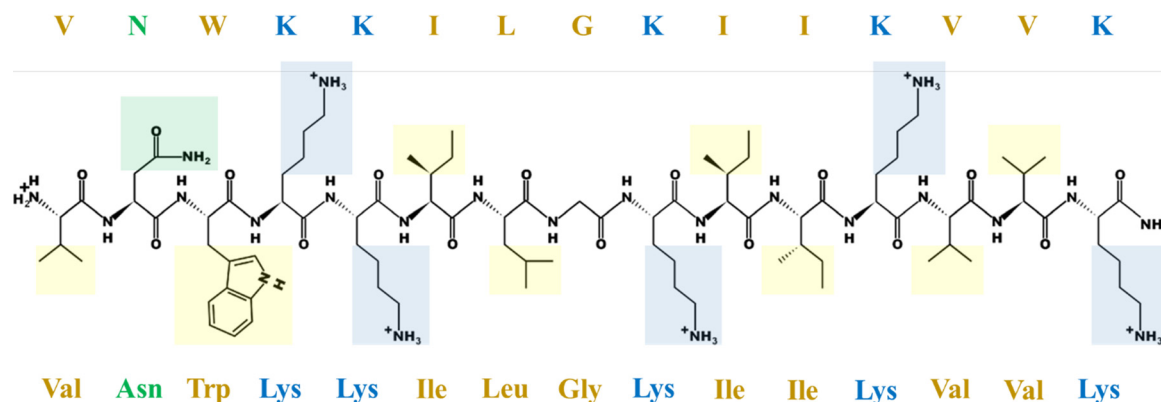


Fig. 1 The LL-III sequence in an extended conformation with amino acid side chains highlighted. The color code is as follows: yellow for hydrophobic, green for polar uncharged, blue for the polar positively charged residues. The peptide structure at pH 6.5 was generated using the online tool "PepDraw" developed by the Tulane University (Louisiana, USA) available at <https://pepdraw.com/>.<sup>10</sup>

some cancer cell lines such as human lymphoblastic leukemia, human promyelocytic leukemia, human cervix carcinoma and human colon adenocarcinoma.<sup>11</sup> Particularly, it has been reported that this peptide can translocate across tumor cell membranes in a non-disruptive manner, suggesting that its action mechanism involves the recognition of one or more intracellular targets.<sup>12</sup> However, the exact mechanism through which the peptide reaches the cell cytoplasm is still unknown. Here, we have biophysically characterized LL-III interaction with model tumor membranes in order to clarify its membrane perturbing effects and to provide a reasonable explanation for the translocation mechanism. We have selected the lipid pair 1-palmitoyl-2-oleoyl-*sn*-glycero-3-phosphatidylcholine (POPC)/1-palmitoyl-2-oleoyl-*sn*-glycero-3-*rac*-phosphoserine (POPS) to mimic the basic characteristics of the tumor membrane lipid matrix. Particularly, we chose POPS as a representative of phosphatidylserines for two main reasons: it is characterized by a  $T_m$  of 14 °C, which guarantees that at room temperature it is in a liquid crystalline phase like POPC<sup>13</sup> and it shows higher miscibility with phosphatidylcholines when compared, for example, to the saturated lipid DPPS.<sup>14,15</sup> Moreover, as the extracellular matrix contains a  $\text{Ca}^{2+}$  concentration of  $\sim 1\text{--}2$  mM and no description of the effects of its coordination to PS lipids on ACP binding is currently available, we performed all our experiments both in the absence and in the presence of a physiological concentration of  $\text{Ca}^{2+}$ .<sup>16</sup> For comparison, the interaction of LL-III with the liposome of POPC/Chol mimicking the normal cell membrane was also studied. In this work, the ability of LL-III to selectively recognize and perturb the model tumor membrane was shown and the effect of  $\text{Ca}^{2+}$  on such interactions was revealed to be only marginal. Our results are compatible with a peptide surface binding mode as no deep penetration into the hydrophobic core has been observed. As shown in our calorimetric data, the main effect of the peptide is to induce lipid membrane lateral reorganization, likely due to the specific interaction with the anionic component PS, which involves the progressive substitution of the coordinated  $\text{Ca}^{2+}$ . These membrane physicochemical property alterations allow LL-III to permeabilize the membrane

(as shown in our leakage experiment), providing an explanation for its translocation mechanism across the tumor membrane. Overall, our data are consistent with the non-membranolytic action mechanism.

## 2. Materials and methods

### 2.1 Materials

The peptide lasioglossin-III (LL-III) with the sequence  $\text{NH}_2\text{-VNWKKILGKIIKVVK-CONH}_2$  was purchased from Primm Srl (Milano, Italy) with a purity of  $>95\%$ . The lipids cholesterol (Chol), 1,2-dipalmitoyl-*sn*-glycero-3-phosphatidylcholine (DPPC), 1-palmitoyl-2-oleoyl-*sn*-glycero-3-phosphatidylserine (POPS) and 1-palmitoyl-2-oleoyl-*sn*-glycero-3-phosphatidylcholine (POPC) as well as spin-labeled phosphatidylcholines used as EPR probes (1-palmitoyl-2-stearoyl-(*n*-doxyl)-*sn*-glycero-3-phosphatidylcholine, *n*PC-SL,  $n = 5, 7, 10$ , and  $14$ ) were provided by Avanti Polar Lipids (Alabaster, United States). The fluorescent probes, 1,6-diphenylhexatriene (DPH) and 6-dodecanoyl-2-dimethylaminonaphthalene (Laurdan), chloroform, methanol, dimethylformamide (DMF), cacodylic acid, calcium chloride ( $\text{CaCl}_2$ ), sodium chloride ( $\text{NaCl}$ ), sodium hydroxide ( $\text{NaOH}$ ) and carboxyfluorescein (CF) were acquired from Merck (Darmstadt, Germany). Sodium cacodylate buffer (10 mM) was prepared by solubilizing cacodylic acid in deionized water and adjusting the pH to 6.5 or 7.0 by adding an appropriate amount of  $\text{NaOH}$ . The pH values of 6.5 and 7.0 were selected to mimic tumor and healthy cell extracellular matrices, respectively.<sup>17</sup>

### 2.2 Liposome preparation

Lipids were weighed in a darkened glass vial and solubilized in a chloroform/methanol mixture (2/1 v/v). A thin layer of an appropriate lipid mixture was obtained by removing the organic solvent with a gentle nitrogen flux. The sample was kept drying under vacuum for at least 4 hours in order to promote the evaporation of the remaining traces of organic solvents. The lipid film was then hydrated by adding sodium cacodylate buffer at the desired pH with or without 1 mM  $\text{CaCl}_2$



at a temperature major than the lipid transition temperature. The sample was vigorously mixed to obtain multilamellar vesicles (MLVs). To incorporate DPH in the lipid vesicles, a solution of the probe in chloroform was added to the lipid mixture in the thin layer formation step at a lipid/DPH mole ratio of 150. The same procedure was employed to prepare vesicles containing Laurdan, by adding a probe solution in DMF to achieve a lipid/Laurdan mole ratio of 30. For electron paramagnetic resonance (EPR) measurements, appropriate aliquots of nPC-SL solution in ethanol (1% w/w) were added to the lipid mixture in organic solvents to obtain 2% mol mol<sup>-1</sup> of spin-labelled phosphatidylcholines over total lipids. When required for the experimental technique, MLVs were extruded at least 27 times through a porous polycarbonate membrane to obtain ~100 nm large unilamellar vesicles (LUVs) using a Mini-Extruder (Avanti Polar Lipids), equipped with two glass syringes of 1 mL. The LUV size was checked by determining the hydrodynamic diameter thanks to dynamic light scattering measurements performed on a Zetasizer Nano ZS from Malvern Instruments (Malvern, United States). LUVs containing carboxy-fluorescein (CF) were prepared by hydrating the lipid film with a solution 40 mM CF in sodium cacodylate buffer and the obtained MLVs were extruded as previously described. The CF in solution was removed by means of gel-filtration, passing the suspension through a G25 Sephadex medium column (1.45 × 5.0 cm). As elution buffer sodium cacodylate 10 mM in the presence of 1 mM CaCl<sub>2</sub> and 150 mM NaCl was employed to prevent the vesicles from disrupting due to osmotic stress. The fractions containing the vesicles were collected and unified. As the procedure involves the loss of lipids, their concentration was determined by performing Stewart assay.<sup>18</sup> The selected compositions to mimic the tumor cell membranes were POPC/POPS 8/2 mol mol<sup>-1</sup> and DPPC/POPS 8/2 mol mol<sup>-1</sup> while POPC/Chol 8:2 mol mol<sup>-1</sup> was used for the healthy eukaryotic cell membrane. The appropriate amounts of a peptide solution were added to the lipid suspensions to obtain the desired lipid to peptide (L/P) mole ratios for the experiments.

### 2.3 Steady-state fluorescence spectroscopy

Fluorescence experiments were performed on a Horiba Fluoromax-4 from Horiba Scientific (Edison, USA) at a controlled temperature of 25 °C and in 10 mM sodium cacodylate buffer at pH 6.5 or 7.0.

**2.3.1 Binding to the model membrane.** To determine the affinity of LL-III towards POPC/POPS 8/2 mol mol<sup>-1</sup> and POPC/Chol 8/2 mol mol<sup>-1</sup> LUVs, Trp emission was monitored upon increasing the total lipid concentration (up to ~1.2 mM). The peptide concentration was fixed at 6.5 μM and the samples were prepared in the presence of 1 mM CaCl<sub>2</sub> or 3 mM NaCl. The excitation wavelength was set to 280 nm and the emission collected between 295 and 450 nm. The slits were set to 6 and 9 nm for the excitation and emission monochromators, respectively. All the spectra were recorded after an equilibration time of 3 minutes in a 1 cm path-length quartz cuvette, under constant stirring. At least three spectra for each sample were recorded until they were superimposable, indicating that

equilibrium was reached. To minimize the spectrum distortion due to excitation radiation scattering caused by the presence of the lipid vesicles, the excitation and emission polarizers were set to 90° and 0°, respectively, as described elsewhere.<sup>19</sup> The binding curve was constructed by reporting the fluorescence intensity at 330 nm (*I*) normalized to the fluorescence intensity of the peptide alone (*I*<sub>0</sub>) as a function of lipid concentration. The binding curve analysis was performed according to a previously described method in order to determine the mole-fraction partition constant using the software Origin Pro 2018 from OriginLab (Northampton, USA).<sup>20</sup>

**2.3.2 Laurdan general polarization.** The emission spectra of Laurdan containing POPC/POPS LUVs were recorded under excitation at 340 nm, collecting the emission from 380 to 600 nm and setting the slits to 3 and 7 nm for the excitation and emission monochromators, respectively. The total lipid concentration was fixed at 50 μM and LL-III was added at increasing concentrations (up to ~55 μM). To improve the signal to noise ratio and reduce the background scattering, all the spectra were recorded in a 1 cm path length cuvette equipped with darkened windows. Each sample was equilibrated for 3 minutes before the measurement and at least three spectra were acquired to assure that the system was in equilibrium and the results were reproducible. The experiments were performed in the presence or the absence of 1 mM CaCl<sub>2</sub>. The Laurdan emission general polarization (GP) was calculated as previously described according to the formula  $GP = (I_{440} - I_{490}) / (I_{440} + I_{490})$ , where *I* is the fluorescence intensity at a specified wavelength.<sup>21</sup> The obtained values were reported as a function of the LL-III concentration. The experiments were performed in triplicates and the average GP and the corresponding mean standard deviation were calculated.

**2.3.3 Anisotropy.** The fluorescence anisotropies of Laurdan and DPH embedded in POPC/POPS LUVs (a total lipid concentration of 50 μM) were recorded upon increasing LL-III concentration (up to ~55 μM). The experiments were performed in the presence or in the absence of 1 mM CaCl<sub>2</sub>. A 1 cm path-length cuvette with darkened windows was employed. DPH was excited at 355 nm and the emission anisotropy was recorded at 425 nm. The excitation monochromator slit was set to 11 nm while the emission monochromator slit was set to 16 nm. Laurdan was excited at 340 nm and the anisotropy was recorded at 476 nm. The excitation and emission monochromator slits were set to 7 and 13, respectively. For each sample, 7 measurements were performed and averaged. Fluorescence millianisotropy (*r*) was calculated by means of the formula:  $10^3 \cdot [(I_{VV} - GI_{VH}) / (I_{VV} + 2GI_{VH})]$ , where the intensity (*I*) first and second subscripts respectively indicate the orientation of the excitation and of the emission polarizer (V, vertical and H, horizontal). *G* is an instrumental correction factor.

**2.3.4 Leakage assay.** Leakage assay was performed on carboxyfluorescein (CF) containing POPC/POPS LUVs in the presence of 1 mM CaCl<sub>2</sub> and 150 mM NaCl as previously described. When entrapped in lipid vesicles at high local concentrations, CF is characterized by a low fluorescence intensity due to self-quenching phenomena. Thus, the leakage





rate was monitored by recording the increase in the dye emission as a function of time. The total lipid concentration was fixed at 2.15  $\mu\text{M}$  and the vesicles were incubated with various LL-III concentrations up to 1350 nM. Each sample had a final volume of 1 mL and was loaded in a 1 cm path-length cuvette. CF was excited at 493 nm and the emission was recorded at 515 nm with excitation and emission monochromator slits both set to 2 nm. The signal related to the condition of 100% leakage was determined by treating the liposome suspension with a solution of 10% Triton X to completely disrupt the vesicles. The leakage percentage was calculated by means of the expression:  $\text{Leakage (\%)} = (I_t - I_0)/(I_{\text{max}} - I_0) \times 100$ , where  $I_t$  is the intensity at time  $t = 1500$  s,  $I_0$  is the initial intensity and  $I_{\text{max}}$  is the intensity after treating the sample with 10% Triton X.

## 2.4 Circular dichroism (CD)

To evaluate the LL-III secondary structure, the far-UV spectra of the peptide at a fixed concentration of 15  $\mu\text{M}$  were recorded using a Jasco 1500 spectropolarimeter from Jasco Corporation (Tokyo, Japan) in the absence or in the presence of POPC/POPS or POPC/Chol LUVs at a L/P ratio of 100. All the samples were prepared in 10 mM sodium cacodylate buffer at pH 6.5 and 1 mM  $\text{CaCl}_2$ . A quartz 0.1 cm path-length cuvette was employed, and the temperature was fixed at 25  $^\circ\text{C}$ . The spectra were recorded between 200 and 260 nm with steps of 0.5 nm, a scan rate of 50 nm  $\text{min}^{-1}$ , a bandwidth of 4.0 nm and a response time of 2 s. Each spectrum was the average of 5 measurements.

## 2.5 Electron paramagnetic resonance spectroscopy (EPR)

The EPR spectra of *n*PC-SL in POPC/POPS MLV suspensions were recorded in the absence or in the presence of LL-III at a L/P mole ratio of 10. The total lipid concentration in each sample was 10 mM. Samples were prepared in 10 mM sodium cacodylate buffer in the absence or in the presence of 1 mM  $\text{CaCl}_2$ . EPR experiments were performed using a 9 GHz Bruker Elexys E-500 spectrometer (Bruker, Rheinstetten, Germany). Capillaries containing the samples ( $\sim 25$   $\mu\text{L}$ ) were placed in a standard 4 mm quartz sample tube. The instrumental settings were as follows: sweep width, 100 G; resolution, 1024 points; modulation frequency, 100 kHz; modulation amplitude, 1.0 G; time constant, 20.5 ms; and incident power, 5.0 mW. Several scans, typically 8, were accumulated to improve the signal-to-noise ratio. A quantitative analysis of *n*PC-SL spectra was performed by determining the acyl chain order parameter,  $S$ , and the nitrogen isotropic hyperfine coupling constant,  $a'_N$ , as described in the literature.<sup>22</sup> The differential order parameters,  $\Delta S$ , and differential nitrogen isotropic hyperfine coupling constants,  $\Delta a'_N$ , were calculated subtracting the values determined for POPC/POPS MLVs alone from the values determined for each sample. The experiments were performed in triplicates.

## 2.6 Differential scanning calorimetry (DSC)

The heat capacity curves of DPPC/POPS vesicles in the absence and or in the presence of LL-III at L/P ratios of 100, 50 and 10

were recorded by means of a nano-DSC equipment from TA Instruments (New Castle, USA) equipped with two twin gold capillary cells of 300  $\mu\text{L}$ . The total lipid concentration in each sample was 500  $\mu\text{M}$  and MLVs were used in all the experiments as the associated calorimetric peaks have a higher resolution.<sup>23</sup> Samples were prepared in 10 mM sodium cacodylate buffer in the absence or in the presence of 1 mM  $\text{CaCl}_2$ . The temperature interval was 25–55  $^\circ\text{C}$  and the scan rate was set to 1  $^\circ\text{C min}^{-1}$ . The capillary cells were subjected to a pressure of 3 atm to prevent bubble formation. A buffer only scan was recorded with the same settings and subtracted from the sample thermograms prior to the calorimetric peak analysis. For each sample, at least four heating and cooling scans were recorded to assess reproducibility and reversibility. The experiments were performed in triplicates and the average  $\Delta H_m$  and  $T_m$  and the standard deviations were calculated.

# 3. Results

## 3.1 Binding of LL-III to model membranes

First, we evaluated the ability of LL-III to bind to the cancer cell model membrane by means of steady-state fluorescence spectroscopy. We monitored the variations in the emission of the LL-III Trp residue upon the addition of POPC/POPS LUVs. In addition, to explore the effect of  $\text{Ca}^{2+}$  on the binding constant, the experiments were performed both in the absence (Fig. 2, panel A) and in the presence (Fig. 2, panel B) of 1 mM of this cation. In the former case, the ionic strength was kept constant by adding 3 mM NaCl.

As shown in Fig. 2, in both cases, an enhancement of fluorescence intensity and a blue shift of about 23 nm were observed upon the addition of POPC/POPS vesicles (at the highest concentration), revealing that the Trp residue experiences a more rigid and hydrophobic environment.<sup>24</sup> These results are consistent with an interaction of the peptide with the POPC/POPS vesicles and further suggest a partial insertion of the peptide into the lipid bilayer. To estimate the effect of  $\text{Ca}^{2+}$  on binding, we evaluated the mole fraction partition constants ( $K_x$ ) in the presence and in the absence of the cation by fitting the corresponding binding isotherms (insets of Fig. 1) as previously reported.<sup>19</sup> Interestingly, the coordination of  $\text{Ca}^{2+}$  to the lipid head groups only marginally affects the partition equilibrium, with a reduction of  $K_x$  from  $6.5 \pm 1.4 \times 10^5$  to  $4.8 \pm 0.7 \times 10^5$ . Overall, the coordination of  $\text{Ca}^{2+}$  to the POPC/POPS membrane does not hamper the LL-III membrane interaction.

We next explored the ability of LL-III to change its conformation upon binding with the POPC/POPS vesicle by means of circular dichroism measurements. Fig. 3 shows the CD spectra of the peptide in the absence and in the presence of lipid vesicles at a lipid to peptide mole ratio L/P of 100 (panel A) and the helical wheel projection of LL-III (panel B).

The examination of the spectra reveals that in the presence of 1 mM  $\text{CaCl}_2$  the peptide is essentially unstructured as observed under neat buffer conditions (Fig. S1, ESI<sup>†</sup>), whereas



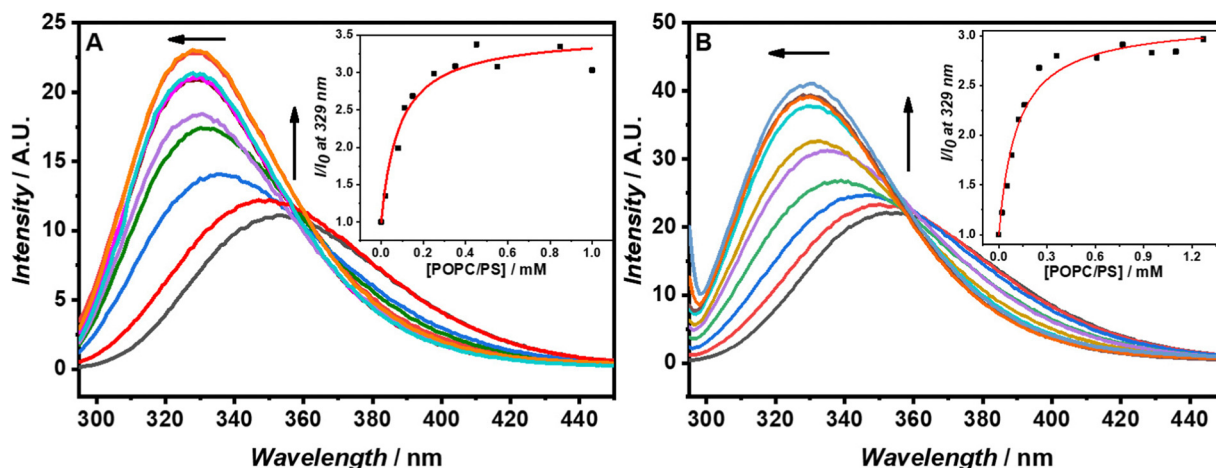


Fig. 2 Fluorescence spectra of LL-III with an increasing concentration of POPC/POPS 8 : 2 LUVs in the presence of 3 mM NaCl (A) and in the presence of 1 mM  $\text{CaCl}_2$  (B). The spectra were recorded at 25 °C in 10 mM sodium cacodylate buffer at pH 6.5. The upward black arrows indicate increasing LUV concentration. The leftward arrows indicate the blue shift of the emission maximum. The insets show the binding curves with the black squares representing the experimental data and the red curve representing the best fit.

in the presence of POPC/POPS vesicles a drastic change of the spectral features is observed. Particularly, upon vesicle addition, a shift of the minimum from 200 nm to about 208 nm is recorded, accompanied by the appearance of a second minimum around 222 nm. In addition, a positive band raises around 200 nm. These changes reveal that LL-III adopts an alpha helical structure upon the interaction with the model membrane. Furthermore, to elucidate the main characteristics of the peptide conformation, we drew the helical wheel projection and calculated the hydrophobic moment  $\mu_H$ , a measure of the structure amphipathicity. Fig. 3 panel B shows that the LL-III polar and hydrophobic residues are well

segregated in the helix ( $\mu_H = 5.93$ ), allowing for an effective interaction with phospholipids to occur at the membrane-water interface.

Finally, for comparison, the interaction of LL-III with POPC/Chol liposomes mimicking the normal cell membrane was also verified. In contrast with POPC/POPS, the addition of POPC/Chol vesicles results in a very small decrease of the fluorescence intensity and no significant wavelength shift (Fig. S2 panel A, ESI†). Furthermore, no conformational changes were observed, suggesting a negligible interaction of LL-III with the eukaryotic-like vesicle (Fig. S2 panel B, ESI†); thus, we did not perform additional experiments with this lipid composition.

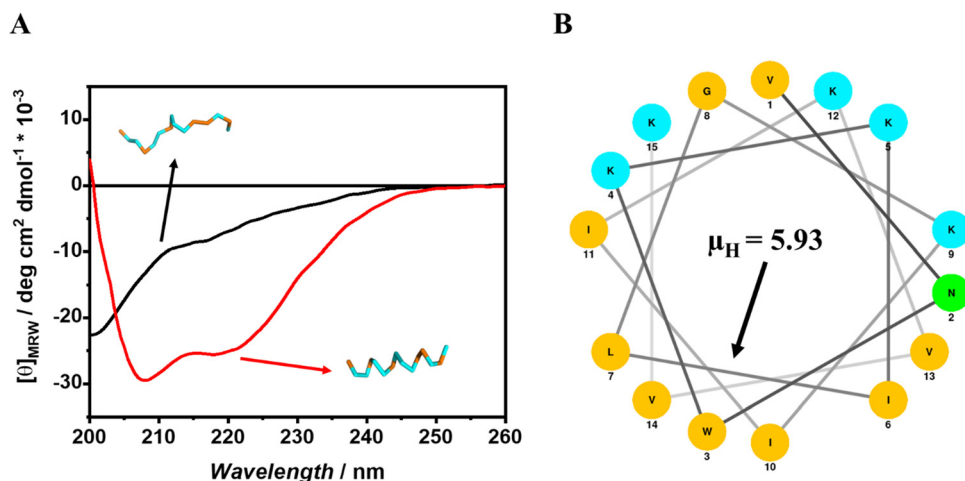


Fig. 3 Far-UV circular dichroism spectra of 15  $\mu\text{M}$  LL-III alone (black curve) and in the presence of POPC/POPS LUVs at a lipid/peptide molar ratio of 100 (red curve). All the spectra were recorded at 25 °C in 10 mM sodium cacodylate buffer at pH 6.5 in the presence of 1 mM  $\text{CaCl}_2$ . The approximate unfolded and folded LL-III structures were built using the software PyMol Version 2.5.2 available at <https://pymol.org/2/> (A).<sup>25</sup> Helical wheel projection of LL-III with the hydrophobic amino acids colored in yellow, polar uncharged amino acids in green and polar positively charged amino acids in blue. The helical wheel projection was constructed using the online tool NetWheels available at <https://netwheels.herokuapp.com/>. The hydrophobic moment  $\mu_H$  was calculated using the software MPEx available on <https://blanco.biomol.uci.edu/mpex> according to the Wimley-White interfacial hydrophobicity scale (B).<sup>26,27</sup>



### 3.2 Effect of LL-III on the lipid bilayer microstructure and hydration properties

To explore in detail the effect of peptide binding on the microstructure of the membrane polar head group region and the hydrophobic core, appropriate fluorescent probes were incorporated in the POPC/POPS LUVs. Particularly, the fluorescent probes Laurdan and DPH were selected as it is known that they partition at the height of glycerol (just below the head group region) and in the hydrophobic core of the bilayer, respectively. Fluorescence anisotropy provides information about the membrane order. Indeed, anisotropy depends on the rotational mobility of the probes and increases if the motion is hindered as an effect of membrane local stiffening. Fig. 4 shows the approximate location of the probes (panel A) and the millianisotropy ( $\langle r \rangle$ ) values of DPH (panel B) and Laurdan (panel C) as a function of the peptide concentration both in the absence and in the presence of  $\text{Ca}^{2+}$ .

Interestingly, upon increasing the LL-III concentration in the absence of  $\text{Ca}^{2+}$ , the anisotropy of both DPH and Laurdan increases, indicating a reduction of the two probes rotational mobility and revealing that the peptide rigidifies the model membrane both in the head group and the hydrophobic core region. Moreover, the increase of DPH anisotropy also suggests that the peptide, most likely, does not penetrate deep into the hydrophobic core of the membrane (otherwise, a reduction of anisotropy should occur, as observed for the membrane penetrating P9Nal(SS) peptide<sup>28</sup>). Similar observations were already reported for the peptide trematocine (which is supposed to act through a carpet mechanism), where an increase of DPH

anisotropy embedded in PC/PG liposomes was observed.<sup>29</sup> Thus, the reported results are compatible with a surface binding mode of LL-III to PC/PS liposomes. Fig. 4, panel C, shows that the trend of Laurdan anisotropy in the presence of  $\text{Ca}^{2+}$  is similar to that observed in the absence of the cation, revealing that the LL-III surface binding mode is not significantly affected by  $\text{Ca}^{2+}$  coordination in the head group region. Remarkably, the increase of the anisotropy for DPH (Fig. 4 panel B) is quite modest in the presence of  $\text{Ca}^{2+}$ , suggesting that the presence of the cation partially counterbalances the rigidification effect of LL-III in the membrane hydrophobic core. Indeed, the millianisotropy values of DPH in the absence and in the presence of  $\text{Ca}^{2+}$  are 113 and 112, respectively, suggesting a slight fluidization effect of calcium of the inner hydrophobic core of the membrane (this effect was also inferred from the EPR data, see Fig. 6, panel A). These results indicate that the cation binding to the head group region increases the probe rotational mobility. This could be due to the induction of a local negative curvature that can increase the spacing among lipid chains. Thus, the almost constant  $r$  of DPH reported in Fig. 4, panel B, can only be due to a counterbalance effect between the peptide (increase of anisotropy) and calcium (decrease of anisotropy).

We next monitored the hydration changes of the lipid head group region taking advantages of the Laurdan emission properties. Indeed, the Laurdan spectra are the result of the emission from two distinct electronic states: a locally excited state, which prevails in hydrophobic environments and is characterized by a higher energy transition and a solvent-relaxed state, which is shifted to lower energies as a

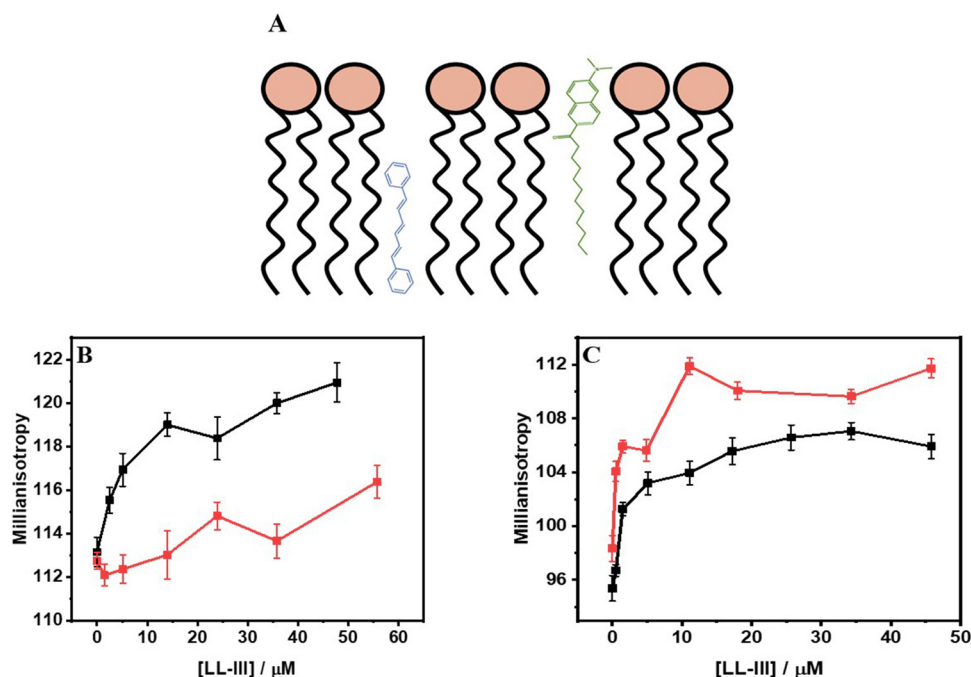


Fig. 4 Schematic representation of Laurdan (in green) and DPH (in blue) locations inside the lipid bilayer (not to scale) (A). Millianisotropy ( $r$ ) values of DPH (B) and Laurdan (C) embedded in POPC/POPS LUVs as a function of the LL-III concentration in the absence (black curves and squares) and in the presence of 1 mM  $\text{Ca}^{2+}$  (red curves and red squares). All the experiments were performed in 10 mM sodium cacodylate buffer at pH 6.5 at 25 °C.



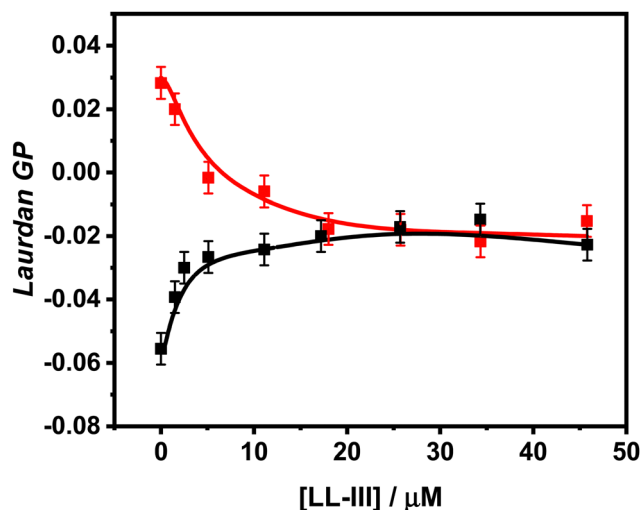


Fig. 5 GP values obtained as described in the Materials and methods section as a function of the LL-III concentration for POPC/POPS LUVs in 10 mM sodium cacodylate buffer at pH 6.5 in the absence (black curve and black squares) and in the presence of 1 mM  $\text{Ca}^{2+}$  (red curve and red circles). Bar errors are the result of error propagation.

consequence of stabilizing solvent interactions.<sup>30</sup> The relative contribution from these two emission states can be quantitatively described by the parameter GP (see Materials and methods section) which provides information on the membrane head group region hydration state. Commonly, the GP values depend on the particular analyzed lipid system in terms of composition and phase and are typically comprised between about 0.6 (less hydrated gel phase) and  $-0.2$  (more hydrated liquid phase).<sup>31</sup> Fig. 5 shows the GP values recorded for Laurdan embedded in POPC/POPS vesicles, upon increasing the LL-III concentration both in the absence and in the presence of  $\text{Ca}^{2+}$ .

In the absence of  $\text{Ca}^{2+}$ , the negative GP value reveals that the model membrane is partially hydrated as expected for a lipid bilayer in the fluid phase. The addition of  $\text{Ca}^{2+}$  leads to a significant dehydration of the membrane surface in agreement with previous studies.<sup>7,9</sup> Upon LL-III addition, the membrane surface hydration state is altered under both conditions but in an opposite way: starting from the  $\text{Ca}^{2+}$  containing sample, LL-III binding results in a partial re-hydration whereas in the absence of the cation it leads to a reduction of the water content. Interestingly, the two curves obtained converge at the highest LL-III concentration suggesting that in the presence of  $\text{Ca}^{2+}$  the peptide progressively replaces the coordinated cation from its binding sites mainly represented by phosphatidylserine head groups. This observation is consistent with a preferential interaction of LL-III with the PS anionic lipid.

To further investigate the effect of LL-III on the lipid bilayer microstructure, an EPR investigation was undertaken. Four spin-labelled phosphatidylcholines bearing the cyclic nitroxide label at various positions along the sn-2 acyl chain ( $n\text{PC-SL}$ ,  $n = 5, 7, 10, 14$ ) were alternatively incorporated in the membrane (2% mol mol<sup>-1</sup> over total lipid). This approach

allows the lipid organization to be investigated in detail as a function of the distance from the bilayer surface. The  $n\text{PC-SL}$  spectra (reported in Fig. S3 and S4, ESI†) were quantitatively analyzed as described in the literature in order to obtain the nitrogen hyperfine coupling constant  $a'_N$ , which is related to the polarity of the microenvironment in which the nitroxide label is embedded, and the order parameter  $S$ , a measure of the orientational ordering of the labelled segment of the acyl chain with respect to the normal to the bilayer surface.<sup>22</sup> The POPC/POPS bilayers present  $S$  and  $a'_N$  profiles typical of membranes in the Ld state.<sup>32</sup> Both parameters decrease with  $n$ , the more dramatic variation being observed for 14PC-SL. Thus, the bilayer inner core is rather disordered and hydrophobic, see Table S1 (ESI†).

Fig. 6 shows the variation of these two parameters due to the presence of LL-III or/and  $\text{Ca}^{2+}$ . The peptide causes an increase of the acyl chain order at all label positions.<sup>33</sup> Particularly, the highest  $\Delta S$  is observed for 5PC-SL, the value becoming lower as the label is stepped down along the acyl chain (Fig. 5, panel A). This evidence clearly points to a peptide positioning at the bilayer interface. The concurrent increase of the local polarity (Fig. 5, panel B) supports this hypothesis and can be ascribed to the polarity of the peptide, which is highly charged, and/or to the peptide hydration which is not completely lost upon membrane interaction.

The adsorption of  $\text{Ca}^{2+}$  ions on the bilayer surface causes opposite effects on lipid ordering depending on the distance from the head group: the positive  $\Delta S$  values are observed for 5 and 7PC-SL, while  $\Delta S$  turns to slightly negative values for 10 and 14PC-SL (Fig. 5, panel A). These evidences suggest that the divalent cations lead to a lipid crowding which results in the stiffening of the more external bilayer section. This perturbation of the lipid organization leaves the tail termini free to move and to assume disordered conformations. No  $\text{Ca}^{2+}$  effect is observed on the  $\Delta a'_N$  profile (Fig. 6, panel B). The expected polarity increase due to the ion interaction could be proposed to be balanced by the bilayer de-hydration observed in the fluorescence experiments.<sup>34</sup>

The effect of LL-III and  $\text{Ca}^{2+}$  seems to be additive in that their simultaneous presence causes the highest increase of the lipid ordering observed in this work. Even in this case, the stronger variations are observed for 5PC-SL, indicating the peptide interaction to occur at the bilayer interface. The peptide determines the  $a'_N$  profile, independent of the  $\text{Ca}^{2+}$  presence.

### 3.3 Effect of LL-III binding on the lipid bilayer thermotropic properties

To further explore the effects of peptide binding on the model membrane physicochemical properties, we performed DSC experiments both in the absence and in the presence of  $\text{Ca}^{2+}$ . As POPC is characterized by a transition temperature below 0 °C, this lipid was replaced by DPPC to obtain a system with a transition temperature suitable for the instrument.<sup>13</sup> The resulting thermograms are shown in Fig. 7. The transition temperatures  $T_m$  and the transition enthalpies  $\Delta H_m$  are listed in Table 1.





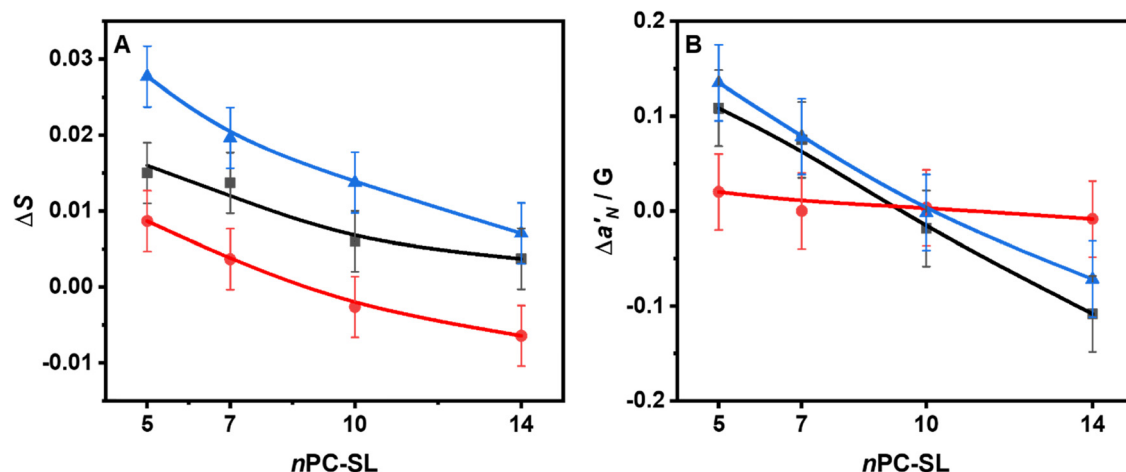


Fig. 6  $\Delta S$  (A) and  $\Delta a'_N$  (B) calculated as described in the Materials and Methods section reported as a function of the spin-label position for POPC/POPS MLVs in the presence of LL-III at a L/P = 10 molar ratio (black curves and squares), in the presence of 1 mM  $\text{CaCl}_2$  (red curves and circles) and in the presence of both LL-III and  $\text{CaCl}_2$  (blue curves and triangles). It is important to note that the reported values for a given system are the difference respect to the values of the probe embedded in the membrane under neat buffer conditions. Bar errors are the mean standard deviations.

The DSC thermogram of DPPC/POPS vesicles under neat buffer conditions is characterized by a broad transition centered at 37.1 °C which is due to the melting of the lipid acyl chain and the associated increase in conformational disorder (Fig. 7, panel A). The addition of  $\text{Ca}^{2+}$  determines the shift of the main transition to higher temperatures and an increase of the transition enthalpy (Table 1 and Fig. 7, panel B). Furthermore, the calorimetric peak is sharper indicating that the lipids melt more cooperatively. Collectively, these data show that  $\text{Ca}^{2+}$  stabilizes the gel phase accordingly with previous studies.<sup>9</sup> Upon LL-III addition, a similar trend was observed both in the presence and in the absence of  $\text{Ca}^{2+}$ : on increasing the peptide concentration, the transition peak is shifted at higher temperatures and the enthalpy progressively decreases (Table 1). At the maximum LL-III concentration employed (L/P 10), the peak shows a double component DSC profile, with

a shoulder extending towards lower temperatures (Fig. 7). The main peak is centered at about 40.4 °C, a temperature which is similar to that of DPPC alone under similar conditions (40.9 °C), suggesting a loss of membrane lateral organization homogeneity due to the formation of lipid domains.<sup>35</sup> This observation is consistent with a preferential interaction of the peptide with the negatively charged PS and the formation of regions enriched in this component which melt at lower temperatures and regions enriched of DPPC which melt at higher temperatures. We further compared the observed  $\Delta T_m$  on increasing the peptide concentration in the absence and in the presence of  $\text{Ca}^{2+}$  (Fig. 8). The trends are very similar and at the maximum LL-III concentration explored the  $\Delta T_m$  values ultimately converge. This result supports the hypothesis that LL-III competes with  $\text{Ca}^{2+}$  for the binding to the PS head group and, at higher concentrations, replaces it.

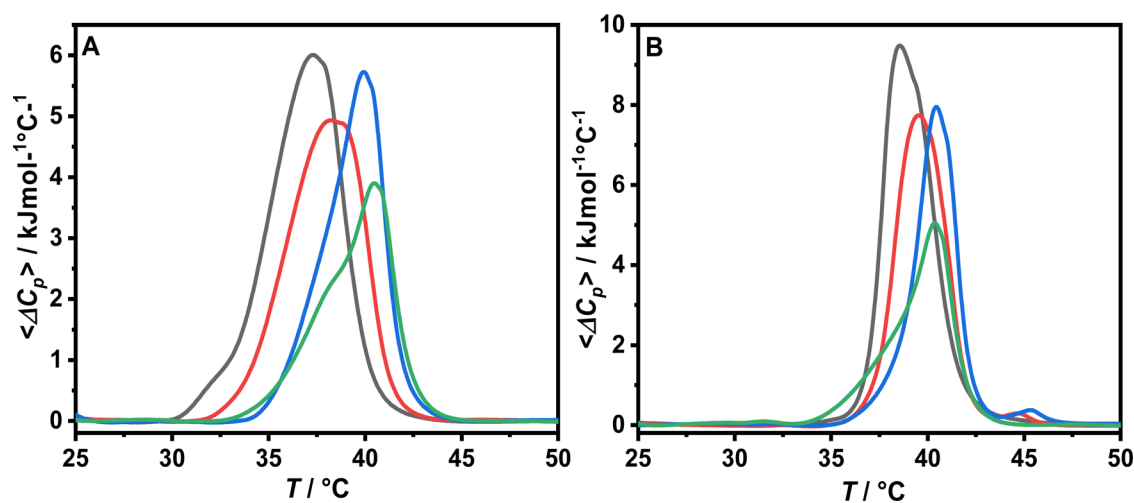
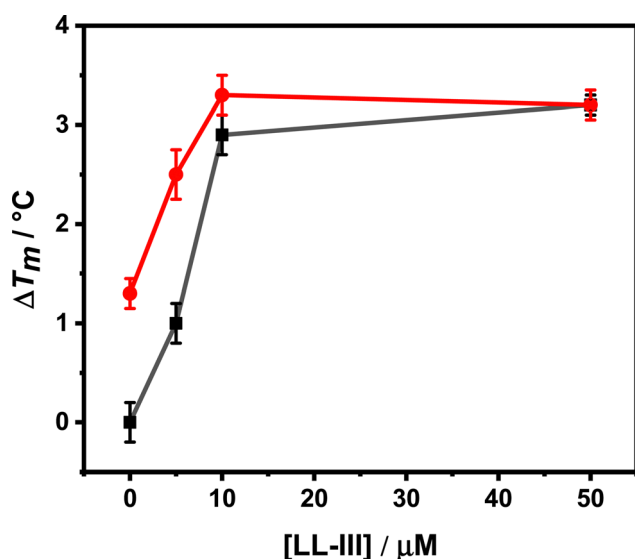


Fig. 7 DSC thermograms of DPPC/POPS 8 : 2 MLVs in 10 mM sodium cacodylate buffer at pH 6.5 in the absence (A) and in the presence of 1 mM  $\text{CaCl}_2$  (B) of the vesicles alone (black curve) and in the presence of LL-III at a L/P ratio of 100 (red curve), 50 (blue curve) and 10 (green curve).



**Table 1** Thermodynamic parameters for 0.5 mM DPPC/POPS 8/2 mol mol<sup>-1</sup> in 10 mM sodium cacodylate buffer at pH 6.5 in the absence and in the presence of LL-III at the indicated L/P ratios with and without the addition of CaCl<sub>2</sub>

| L/P ratio | Buffer                               |            | +1 mM CaCl <sub>2</sub>              |            |
|-----------|--------------------------------------|------------|--------------------------------------|------------|
|           | $\Delta H_m$ (kJ mol <sup>-1</sup> ) | $T_m$ (°C) | $\Delta H_m$ (kJ mol <sup>-1</sup> ) | $T_m$ (°C) |
| /         | 28.8 ± 0.9                           | 37.1 ± 0.2 | 30.2 ± 2.6                           | 38.5 ± 0.1 |
| 100       | 25.1 ± 1.6                           | 38.1 ± 0.2 | 26.0 ± 0.6                           | 39.5 ± 0.3 |
| 50        | 21.8 ± 1.4                           | 39.9 ± 0.2 | 22.4 ± 1.1                           | 40.4 ± 0.2 |
| 10        | 16.7 ± 0.5                           | 40.5 ± 0.1 | 18.2 ± 2.3                           | 40.4 ± 0.1 |



**Fig. 8** Plot of  $\Delta T_m$  as a function of the LL-III concentration. The black curve and black squares refer to the DSC experiments performed in 10 mM sodium cacodylate buffer at pH 6.5. The red curve and red circles refer to the system where 1 mM CaCl<sub>2</sub> was added. Bar errors represent the mean standard deviation.

### 3.4 LL-III effects on membrane permeability

Next, as our data suggest that LL-III does not disrupt the model membrane, we have evaluated its ability to permeabilize the lipid bilayer in the presence of Ca<sup>2+</sup>. To this end, we have performed leakage assay by encapsulating 30 mM carboxyfluorescein (CF) into POPC/POPS LUVs. At a high local concentration, the CF emission is self-quenched.<sup>36</sup> This allows its release in solution to be monitored by following the fluorescence enhancement as a function of time both in the absence and in the presence of an increasing peptide concentration. The kinetic curves and the leakage percentage at 1500 s are reported in Fig. 9. In the absence of LL-III, the fluorescence signal is steady and low due to the self-quenching of the entrapped CF (Fig. 9, panel A). The profile of the recorded kinetic curves is significantly dependent on the peptide concentration added, a feature more consistent with a transient permeabilization rather than equilibrium pore formation.<sup>37</sup> To compare the data at the various peptide concentrations employed, the leakage percentage at 1500 s was reported (Fig. 9, panel B). 50% leakage was observed at a LL-III concentration of

126 nM, corresponding to a bound peptide to lipid mole ratio of 1 : 1000. Therefore, LL-III is able to exert a permeabilizing effect on the model membrane even at a low bound concentration.

## 4. Discussion

LL-III is an antimicrobial and anticancer peptide and has the ability to translocate across tumor cell membranes, probably according to a non-membranolytic action mechanism. However, the molecular basis of the interaction of LL-III with pathogenic membranes and the mechanism through which it gains access to the cell cytoplasm are still unknown. In this paper, a series of physico-chemical techniques have been used to fully characterize the interaction of the anticancer LL-III peptide with the model tumor membrane and the effect of the peptide on the membrane microstructure and thermotropic properties. To mimic the negatively charged surface of tumor cell membranes, we modelled the lipid matrix using POPC/POPS liposomes.<sup>6</sup> Moreover, as the extracellular matrix contains a millimolar concentration of Ca<sup>2+</sup>,<sup>16</sup> which is known to preferentially interact with phosphatidylserines altering lipid bilayer properties,<sup>7,9</sup> the effect of this ion on the LL-III interaction was explored by performing the experiments in the absence and in the presence of Ca<sup>2+</sup>. In addition, the effects of LL-III on POPC/Chol liposomes mimicking healthy cell membrane were also investigated for comparison. The results of the steady-state fluorescence experiments clearly show that the peptide selectively interacts with the POPC/POPS membrane and the presence of Ca<sup>2+</sup> has a negligible effect on the partition constant. Furthermore, Trp emission (Fig. 2) is enhanced and blue shifted upon lipid addition, revealing that this residue is partially inserted into the membrane and suggesting that LL-III partitions at the water-membrane interface. Furthermore, CD experiments show that upon vesicle binding the peptide partially adopts an  $\alpha$ -helical structure upon membrane interactions which involves the segregation of polar and hydrophobic residues on different faces of the structure ( $\mu_H = 5.93$ ). This feature is common with other active anticancer peptides in which the adoption of an amphipathic alpha helical structure favors the interaction with the target membrane.<sup>38</sup> To obtain additional information on the peptide binding mode, we monitored the effect of the peptide on different regions of the membrane by following the changes in the fluorescence anisotropy of the two probes Laurdan and DPH embedded in the lipid bilayer. Specifically, Laurdan provides information on the membrane surface dynamical properties whereas DPH mainly reflects the hydrophobic core of the membrane. Our results clearly show that peptide binding induces a rigidification of the membrane both in the absence and in the presence of Ca<sup>2+</sup>, suggesting that the peptide is, most likely, localized on the membrane surface at the water-membrane interface and does not penetrate deeply in the membrane hydrophobic core. This hypothesis was further supported by EPR measurements showing that the magnitude of peptide-induced rigidification reduces moving from the surface to the lipid acyl chain termini. Interestingly, DPH anisotropy



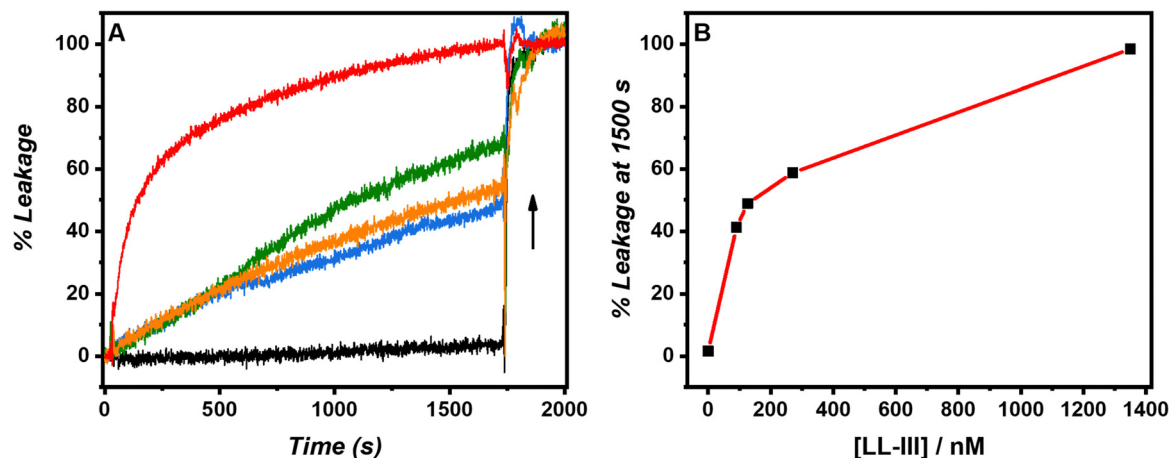


Fig. 9 % Leakage as a function of time. The upward arrow indicated the increasing LL-III concentration (A). Leakage percentage at 1500 s calculated as described in the Materials and methods section as a function of the LL-III concentration (B). Lipid concentration was fixed at 2.15  $\mu\text{M}$ . All the experiments were performed in 10 mM sodium cacodylate buffer at pH 6.5 in the presence of 1 mM  $\text{CaCl}_2$  and 150 mM NaCl at 25  $^\circ\text{C}$ .

appears to be less sensitive to the addition of LL-III in the presence of  $\text{Ca}^{2+}$  (Fig. 4, panel B), suggesting that the presence of the cation partially counterbalances the rigidification effect of LL-III in the hydrophobic region of the membrane. The increase of the probe rotational mobility could be due to a local negative curvature induced by cation coordination which results in an increase of spacing between the lipid acyl chain and in a reduction of the order parameter as sensed by the EPR probe 14-PCSL. Indeed, previous studies have shown that the presence of  $\text{Ca}^{2+}$  at sub-millimolar and millimolar bulk concentrations can induce the formation of invaginations on the surface of membranes containing anionic lipids (*e.g.* DOPE/DOPS bilayers)<sup>40</sup> as a consequence of lipid clustering and of a reduction of the spontaneous curvature.<sup>39</sup> The Laurdan GP measurement in the presence and absence of  $\text{Ca}^{2+}$  allowed us to monitor the hydration state of the membrane surface on increasing the peptide concentration. We found that in the absence of LL-III the hydration of the membrane is very different after the addition of  $\text{Ca}^{2+}$ , being much more dehydrated compared to the neat buffer. Despite this difference, the addition of the peptide leads to a bound state under both conditions showing a very similar GP value, suggesting that LL-III preferentially interacts with PS and progressively substitutes the coordinated  $\text{Ca}^{2+}$  from its binding sites. To verify the ability of the peptide to preferentially bind the anionic lipids, we monitored the effect of peptide addition on the thermotropic properties of DPPC/POPS vesicles by means of DSC measurements. The examination of the DSC profiles shows that LL-III turns the single component DSC profile of DPPC/POPS into a multicomponent DSC profile, which consists of two overlapping peaks, indicating phase segregation. This observation is fully consistent with a preferential interaction of the peptide with the lipid anionic component resulting in a lateral redistribution of membrane lipids and domain formation. Overall, the calorimetric, EPR and fluorescence data clearly reveal that LL-III binds on the membrane surface and does not significantly perturb the membrane integrity, indicating a non-membranolytic action

mechanism (*i.e.*, a mechanism that does not involve permanent damages in the membrane as a cause of cell death),<sup>41</sup> in agreement with the previously reported data showing that the tumor cell membrane is still intact after peptide translocation into the cytoplasm.<sup>12</sup> In addition, we can speculate about the peptide binding mode. Starting from the peptide helical projection (Fig. 3 panel B) and assuming that the helix is oriented parallel on the membrane surface with its hydrophobic side (where Trp occupies a central position) pointing to the membrane hydrophobic core, we suggest that Lys<sup>4</sup>, Lys<sup>9</sup> and Lys<sup>15</sup> are the amino acids most likely involved in an electrostatic interaction with PS head groups whereas Lys<sup>5</sup> and Lys<sup>12</sup> probably interact with water molecules.

Then, we evaluated the ability of the peptide to permeabilize the membrane by performing a leakage assay after encapsulating carboxyfluorescein in the lipid vesicles. Our data (Fig. 9) indicate that LL-III favors the release of the vesicle content with a concentration-dependent rate and plateau level, which is compatible with membrane permeabilization due to a transient and local bilayer destabilization,<sup>37</sup> rather than a true equilibrium pore formation which would lead to the complete loss of the vesicles content even at the lowest peptide concentration employed.<sup>42</sup> We propose that this effect is a consequence of the clustering of anionic lipids promoted by peptide binding. Indeed, the presence of packing irregularities at the lipid domain boundaries can locally lower the permeability barrier allowing LL-III translocation into the cancer cell cytoplasm.<sup>43</sup>

In summary, we performed detailed biophysical characterization of the interaction of LL-III with a lipid bilayer containing the anionic lipid phosphatidylserine and in the presence of a physiological concentration of  $\text{Ca}^{2+}$ . Overall, our data are consistent with the observed non-membranolytic activity of LL-III. In addition, we showed that the presence of calcium (at a physiologically relevant concentration) has only minor effects on the LL-III mechanism of action. Furthermore, the obtained results provide a molecular level description of the interaction of the peptide with a lipid bilayer mimicking the



lipid matrix of a tumor cell membrane, and such information can be useful in the development of new peptides that can act as anticancer agents.

## Abbreviations

|         |   |
|---------|---|
| ACPs    | Anticancer peptides   |
| CD      | Circular dichroism  |
| CF      | Carboxyfluorescein  |
| Chol    | Cholesterol   |
| DMF     | Dimethylformamide   |
| DPH     | 1,6-Diphenylhexatriene  |
| DPPC    | 1,2-Dipalmitoyl- <i>sn</i> -glycero-3-phosphatidylcholine                           |
| DSC     | Differential scanning calorimetry   |
| EPR     | Electron paramagnetic resonance   |
| GP      | General polarization  |
| HDPs    | Host defense peptides   |
| Laurdan | 6-Dodecanoyl-2-dimethylaminonaphthalene   |
| LL-III  | Lasioglossin-III  |
| LUVs    | Large unilamellar vesicles  |
| MLVs    | Multilamellar vesicles  |
| nPC-SL  | 1-Palmitoyl-2-stearoyl-( <i>n</i> -doxyl)- <i>sn</i> -glycero-3-phosphatidylcholine |
| POPC    | 1-Palmitoyl-2-oleoyl- <i>sn</i> -glycero-3-phosphatidylcholine                      |
| POPS    | 1-Palmitoyl-2-oleoyl- <i>sn</i> -glycero-3-rac-phosphoserine                        |
| PS      | Phosphatidylserine  |

## Conflicts of interest

There are no conflicts of interest to declare.

## Acknowledgements

The authors are grateful to the Italian MUR for granting Rosario Oliva with a research associated position (PON R&I 2014-2020, CUP: E65F21003250003).

## References

- 1 R. L. Siegel, K. D. Miller, H. E. Fuchs and A. Jemal, Cancer statistics, *Ca-Cancer J. Clin.*, 2022, **72**, 7–33.
- 2 F. Harris, S. R. Dennison, J. Singh and D. A. Phoenix, On the selectivity and efficacy of defense peptides with respect to cancer cells, *Med. Res. Rev.*, 2013, **33**, 190–234.
- 3 R. E. Hancock and G. Diamond, The role of cationic antimicrobial peptides in innate host defences, *Trends Microbiol.*, 2000, **8**, 402–410.
- 4 M. Xie, D. Liu and Y. Yang, Anti-cancer peptides: classification, mechanism of action, reconstruction and modification, *Open Biol.*, 2020, **10**, 200004.
- 5 D. Gaspar, A. S. Veiga and M. A. R. B. Castanho, From antimicrobial to anticancer peptides. A review, *Front. Microbiol.*, 2013, **4**, 1–16.
- 6 W. Chiangjong, S. Chutipongtanate and S. Hongeng, Anti-cancer peptide: Physicochemical property, functional aspect and trend in clinical application (Review), *Int. J. Oncol.*, 2020, **57**, 678–696.
- 7 A. Melcrová, S. Pokorna, S. Pullanchery, M. Kohagen, P. Jurkiewicz, M. Hof, P. Jungwirth, P. S. Cremer and L. Cwiklik, The complex nature of calcium cation interactions with phospholipid bilayers, *Sci. Rep.*, 2016, **6**, 38035.
- 8 M. L. Valentine, A. E. Cardenas, R. Elber and C. R. Baiz, Calcium-Lipid Interactions Observed with Isotope-Edited Infrared Spectroscopy, *Biophys. J.*, 2020, **118**, 2694–2702.
- 9 A. Melcrová, S. Pokorna, M. Vošahlíková, J. Sýkora, P. Svoboda, M. Hof, L. Cwiklik and P. Jurkiewicz, Concurrent Compression of Phospholipid Membranes by Calcium and Cholesterol, *Langmuir*, 2019, **35**, 11358–11368.
- 10 PepDraw: a tool to draw peptide primary structure and calculate theoretical properties, accessed November 2, 2022, <https://pepdraw.com/>.
- 11 V. Cеровský, M. Budesínský, O. Hovorka, J. Cvacka, Z. Voburka, J. Slaninová, L. Borovicková, V. Fucík, L. Bednářová, I. Votruba and J. Straka, Lasioglossins: three novel antimicrobial peptides from the venom of the eusocial bee *Lasioglossum laticeps* (Hymenoptera: Halictidae), *ChemBioChem*, 2009, **10**, 2089–2099.
- 12 J. Slaninová, V. Mlsová, H. Kroupová, L. Alán, T. Tůmová, L. Monincová, L. Borovicková, V. Fučík and V. Ceřovský, Toxicity study of antimicrobial peptides from wild bee venom and their analogs toward mammalian normal and cancer cells, *Peptides*, 2012, **33**, 18–26.
- 13 Phase Transition Temperatures for Glycerophospholipids, <https://avantilipids.com/tech-support/physical-properties/phase-transition-temps>, accessed November 4, 2022.
- 14 Miscibility of Phospholipid Binary Mixtures, <https://avantilipids.com/tech-support/physical-properties/miscibility>, (accessed November 4, 2022).
- 15 A. Hinderliter, R. L. Biltonen and P. F. F. Almeida, Lipid Modulation of Protein-Induced Membrane Domains as a Mechanism for Controlling Signal Transduction, *Biochemistry*, 2004, **43**, 7102–7110.
- 16 B. Alberts, *Molecular biology of the cell*, W. W. Norton & Company, New York, 7th edn, 2022.
- 17 V. Estrella, T. Chen, M. Lloyd, J. Wojtkowiak, H. H. Cornell, A. Ibrahim-Hashim, K. Bailey, Y. Balagurunathan, J. M. Rothberg, B. F. Sloane, J. Johnson, R. A. Gatenby and R. J. Gillies, Acidity Generated by the Tumor Microenvironment Drives Local Invasion, *Cancer Res.*, 2013, **73**, 1524–1535.
- 18 J. C. M. Stewart, Colorimetric determination of phospholipids with ammonium ferrothiocyanate, *Anal. Biochem.*, 1980, **104**, 10–14.
- 19 A. S. Ladokhin, S. Jayasinghe and S. H. White, How to measure and analyze tryptophan fluorescence in membranes properly, and why bother?, *Anal. Biochem.*, 2000, **285**, 235–245.
- 20 S. H. White, W. C. Wimley, A. S. Ladokhin and K. Hristova, Protein folding in membranes: determining energetics of peptide-bilayer interactions, *Methods Enzymol.*, 1998, **295**, 62–87.





- 21 T. Parasassi and E. Gratton, Membrane lipid domains and dynamics as detected by Laurdan fluorescence, *J. Fluoresc.*, 1995, **5**, 59–69.
- 22 S. Galdiero, A. Falanga, G. Vitiello, M. Vitiello, C. Pedone, G. D'Errico and M. Galdiero, Role of membranotropic sequences from herpes simplex virus type I glycoproteins B and H in the fusion process, *Biochim. Biophys. Acta, Biomembr.*, 2010, **1798**, 579–591.
- 23 R. L. Biltonen and D. Lichtenberg, The use of differential scanning calorimetry as a tool to characterize liposome preparations, *Chem. Phys. Lipids*, 1993, **64**, 129–142.
- 24 J. R. Lakowicz, *Principles of fluorescence spectroscopy*, Springer, New York, 3rd edn, 2006.
- 25 L. Schrödinger and W. DeLano, The PyMOL Molecular Graphics System (Version 2.5.2).
- 26 A. R. Mól, M. S. Castro and W. Fontes, NetWheels: A web application to create high quality peptide helical wheel and net projections, *Bioinformatics*, 2018, 416347.
- 27 C. Snider, S. Jayasinghe, K. Hristova and S. H. White, MPEx: A tool for exploring membrane proteins: MPEx: A Tool for Exploring Membrane Proteins, *Protein Sci.*, 2009, **18**, 2624–2628.
- 28 R. Oliva, M. Chino, K. Pane, V. Pistorio, A. De Santis, E. Pizzo, G. D'Errico, V. Pavone, A. Lombardi, P. Del Vecchio, E. Notomista, F. Natri and L. Petraccone, Exploring the role of unnatural amino acids in antimicrobial peptides, *Sci. Rep.*, 2018, **8**, 8888.
- 29 G. Della Pelle, G. Perà, M. C. Belardinelli, M. Gerdol, M. Felli, S. Crognale, G. Scapigliati, F. Ceccacci, F. Buonocore and F. Porcelli, Trematocine, a Novel Antimicrobial Peptide from the Antarctic Fish *Trematomus bernacchii*: Identification and Biological Activity, *Antibiotics*, 2020, **9**, 66.
- 30 K. Gaus, T. Zech and T. Harder, Visualizing membrane microdomains by Laurdan 2-photon microscopy (Review), *Mol. Membr. Biol.*, 2006, **23**, 41–48.
- 31 T. Parasassi, G. De Stasio, G. Ravagnan, R. M. Rusch and E. Gratton, Quantitation of lipid phases in phospholipid vesicles by the generalized polarization of Laurdan fluorescence, *Biophys. J.*, 1991, **60**, 179–189.
- 32 G. Vitiello, A. Falanga, A. Alcides Petruk, A. Merlino, G. Fragneto, L. Paduano, S. Galdiero and G. D'Errico, Fusion of raft-like lipid bilayers operated by a membranotropic domain of the HSV-type I glycoprotein gH occurs through a cholesterol-dependent mechanism, *Soft Matter*, 2015, **11**, 3003–3016.
- 33 R. Oliva, A. Emendato, G. Vitiello, A. De Santis, M. Grimaldi, A. M. D'Ursi, E. Busi, P. Del Vecchio, L. Petraccone and G. D'Errico, On the microscopic and mesoscopic perturbations of lipid bilayers upon interaction with the MPER domain of the HIV glycoprotein gp41, *Biochim. Biophys. Acta, Biomembr.*, 2016, **1858**, 1904–1913.
- 34 H. A. Hussain, The effect of cation concentration on the nitrogen splitting constant of nitroxide free radicals, *Collect. Czech. Chem. Commun.*, 1990, **55**, 2377–2380.
- 35 F. Battista, R. Oliva, P. Del Vecchio, R. Winter and L. Petraccone, Insights into the Action Mechanism of the Antimicrobial Peptide Lasioglossin III, *Int. J. Mol. Sci.*, 2021, **22**, 2857.
- 36 Y. N. Antonenko, G. S. Gluhov, A. M. Firsov, I. D. Pogozheva, S. I. Kovalchuk, E. V. Pechnikova, E. A. Kotova and O. S. Sokolova, Gramicidin A disassembles large conductive clusters of its lysine-substituted derivatives in lipid membranes, *Phys. Chem. Chem. Phys.*, 2015, **17**, 17461–17470.
- 37 W. C. Wimley and K. Hristova, The Mechanism of Membrane Permeabilization by Peptides: Still an Enigma, *Aust. J. Chem.*, 2020, **73**, 96–103.
- 38 S. R. Dennison, M. Whittaker, F. Harris and D. A. Phoenix, Anticancer alpha-helical peptides and structure/function relationships underpinning their interactions with tumour cell membranes, *Curr. Protein Pept. Sci.*, 2006, **7**, 487–499.
- 39 C. Allolio and D. Harries, Calcium Ions Promote Membrane Fusion by Forming Negative-Curvature Inducing Clusters on Specific Anionic Lipids, *ACS Nano*, 2021, **15**, 12880–12887.
- 40 Z. T. Graber, Z. Shi and T. Baumgart, Cations induce shape remodeling of negatively charged phospholipid membranes, *Phys. Chem. Chem. Phys.*, 2017, **19**, 15285–15295.
- 41 V. Teixeira, M. J. Feio and M. Bastos, Role of lipids in the interaction of antimicrobial peptides with membranes, *Prog. Lipid Res.*, 2012, **51**, 149–177.
- 42 W. C. Wimley, Describing the Mechanism of Antimicrobial Peptide Action with the Interfacial Activity Model, *ACS Chem. Biol.*, 2010, **5**, 905–917.
- 43 R. F. Epand, G. Wang, B. Berno and R. M. Epand, Lipid Segregation Explains Selective Toxicity of a Series of Fragments Derived from the Human Cathelicidin LL-37, *Antimicrob. Agents Chemother.*, 2009, **53**, 3705–3714.

